10.1098/rsta.2002.1043

THE ROYAL SOCIETY

X-ray spectroscopy of astrophysical plasmas

By Steven M. Kahn, Ehud Behar, Ali Kinkhabwala and Daniel W. Savin

Columbia Astrophysics Laboratory, Columbia University, 550 W. 120th Street, New York, NY 10027, USA

Published online 26 July 2002

We provide a qualitative review of key X-ray spectral diagnostics of astrophysical plasmas. We begin with a brief discussion of the two major types of equilibria, collisional ionization and photoionization, and then consider the behaviour of hydrogen-like, helium-like, iron L-shell and iron K-shell transitions for these separate cases. Where possible, we discuss explicit examples using high-resolution spectra acquired by the grating instruments on the Chandra and XMM-Newton observatories.

Keywords: X-ray spectra; X-ray sources; atomic transitions; temperature diagnostics; density diagnostics

1. Introduction

The science of X-ray astronomy was born in 1962 with the serendipitous discovery of the very bright X-ray binary source, Scorpius X-1 (Giacconi *et al.* 1962). In the ensuing 40 years, this field has progressed to the point where it is now one of the 'standard' disciplines of observational astrophysics (see Pounds (2002) and the other papers in this issue). X-ray observatories have revealed a diverse collection of sources ranging from the nearest stars to the most distant galaxies in the Universe.

However, until very recently, X-ray spectroscopy of astrophysical sources has been largely unavailable, due to instrumental limitations. Non-dispersive detectors, chosen for their high quantum efficiency and large collecting area in most early missions, provided only crude spectral resolution, insufficient for the unambiguous identification of discrete features. As in other wavebands, spectroscopy is crucial to the derivation of quantitative constraints on physical conditions in the sources under investigation.

Within the past two years, this need has finally been met, due to the launches of two major space-observatory facilities. The Chandra X-Ray Observatory, launched by NASA in July 1999, carries two separate transmission-grating spectrometers (Brinkman *et al.* 2000; Canizares *et al.* 2000), collectively providing high-resolution spectra over the broad wavelength band 1–200 Å (0.05–10 keV). The XMM-Newton Observatory, launched by the ESA in December 1999, incorporates reflection-grating spectrometers behind two of the three grazing incidence telescopes carried on board (den Herder *et al.* 2001). These provide high throughput and high resolution in the range 5–38 Å (0.3–2.5 keV). Together, these instruments are providing magnificent spectra of nearly all classes of astrophysical X-ray sources.

One contribution of 15 to a Discussion Meeting 'X-ray astronomy in the new millennium'.

X-ray spectroscopy is very important for astronomy, because X-ray-emitting gas is often the key component of the system. For many objects (e.g. elliptical galaxies, clusters of galaxies), the 'virial temperature' $kT \sim GMm_{\rm p}/R$ lies in the range 10^6–10^8 K, where most of the emission comes out at X-ray energies. In others (e.g. supernova remnants, binary sources), shocks heat gas into the same temperature regime.

In addition, the conventional X-ray band (0.1–10 keV) is unusually rich in discrete spectral features: the K-shell transitions of carbon through iron and the L-shell transitions of silicon through iron fall in this range. In contrast to other wavebands, all charge states are visible in a single X-ray spectrum. This makes the interpretation of the spectrum fairly unambiguous. For example, one can derive relative elemental abundances without invoking any assumptions about the thermal state of the gas.

Finally, because of the high radiative decay rates of X-ray transitions, astrophysical emitting plasmas are generally not in local thermodynamic equilibrium (LTE), except at very high densities (e.g. in the photospheres of neutron stars and white dwarfs). This means that the details of the observed spectra are characterized by the explicit balance between the various microphysical processes that feed and deplete the relevant quantum levels. While that can occasionally lead to complications in the interpretation of the data, it also implies that they are quite sensitive to physical conditions in the source. Hence, X-ray spectra have high diagnostic utility.

2. Types of equilibria

As indicated above, astrophysical X-ray-emitting plasmas are rarely in LTE. Nevertheless, other types of equilibrium can apply. The detailed characteristics of the X-ray spectra depend crucially on the nature of these equilibria. Two cases are especially important.

Collisional equilibrium. Here, the excitations and ionizations are dominated by electron–ion collisions. The electrons are hot, with characteristic temperatures comparable with the energies of the spectral lines observed. The emergent spectrum is nearly a unique function of the electron temperature distribution and the elemental abundances. These conditions apply in stellar coronae, in the intracluster media of clusters of galaxies, in elliptical galaxies, and in the shocked gas in older supernova remnants.

Photoionization equilibrium. In this case, the presence of an intense continuum radiation field has a significant effect on the ionization and thermal structure of the surrounding gas. The electrons are generally too cool to excite prominent X-ray lines. Instead, excited levels are populated by direct recombination and by radiative cascades following recombination onto higher levels, and by direct photoexcitation from the continuum. These conditions can apply in the circumsource media of accretion-powered sources, such as X-ray binaries and active galactic nuclei.

The principal spectroscopic differences between collisionally ionized and photoionized plasmas are due to the very different electron temperatures that accompany a given charge state in the two cases. For collisional ionization, the electron temperature is comparable with the ionization potential, while for photoionization, the photon field does most of the work, so the electron temperature can be much lower.

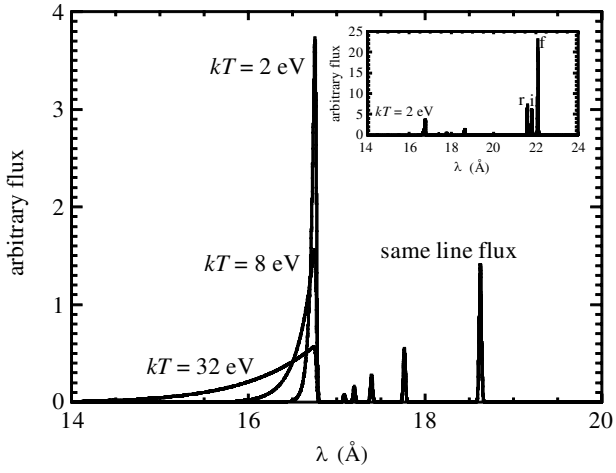

Figure 1. The shape of the radiative recombination continua for recombination forming helium-like oxygen as a function of temperature, assuming the same recombination rate for each temperature.

For example, the characteristic temperature for helium-like oxygen (O^{6+}) in a collisional plasma is $kT_e \sim 100$ eV (Mazzotta *et al.* 1998), whereas the same ion is found in photoionized plasmas at $kT_e \sim 8$ eV (Kallman & Bautista 2001).

Perhaps the most useful spectroscopic diagnostics for distinguishing collisional ionization from photoionization are radiative recombination continua (RRC) (see Liedahl 1999). Radiative recombination generates continua associated with decay from a Maxwellian electron distribution into individual discrete levels. The emission 'turns on' at the ionization energy threshold χ for a particular level and falls off smoothly toward higher energies, with a characteristic width *ca.* kT_e. In a collisional plasma, $kT_e \sim \chi$, so the RRC are broad and have low contrast. On the other hand, in a photoionized plasma, $kT_e \ll \chi$. The RRC are strong and fall off steeply with increasing energy, or decreasing wavelength.

This effect is illustrated in figure 1, where we have plotted the emergent spectrum for pure recombination in helium-like oxygen as a function of the electron temperature. The RRC is the central prominent feature in the plot, with a threshold near 16.8 Å. As can be seen, as the electron temperature increases, this feature grows broader, decreasing its contrast with respect to the accompanying discrete line emission. For a collisionally ionized plasma, the RRC is so broad that it is virtually invisible.

In figure 2, we show the spectrum of the bright Seyfert 2 galaxy NGC 1068, as obtained with the reflection-grating spectrometer on XMM-Newton (Kinkhabwala *et al.* 2002*a*). As can be seen, the spectrum is rich in emission lines, especially hydrogen-like and helium-like lines of low-Z metals (carbon, nitrogen, oxygen and neon). The features labelled RRC in figure 2 are the radiation recombination continua from each of these ions. They are narrow, indicating a low electron temperature of a few eV, characteristic of a photoionized plasma. In NGC 1068, the soft-X-ray spectrum is produced in an ionization cone, which is irradiated by an intense X-ray continuum emanating from a central obscured nucleus.

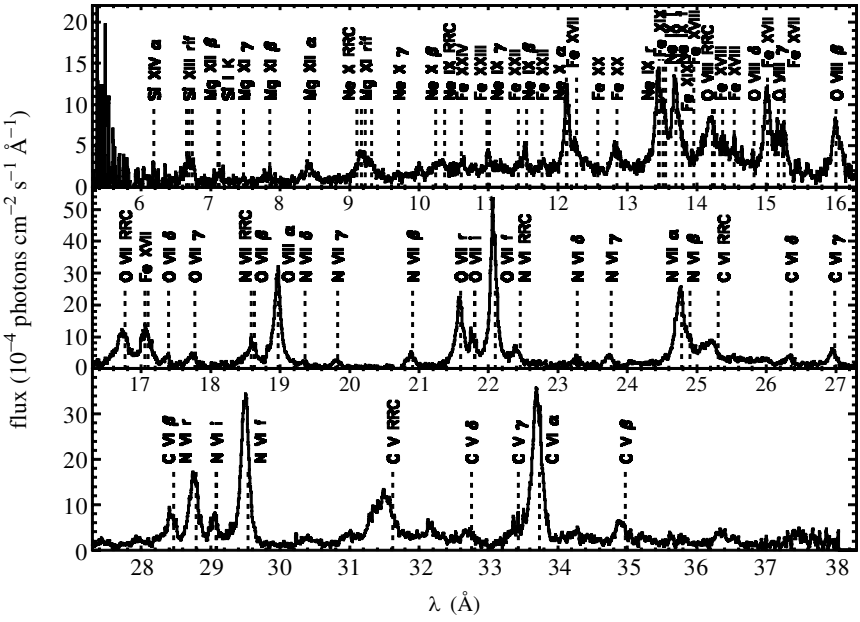

Figure 2. XMM-Newton reflection-grating spectrum of the prototypical Seyfert 2 galaxy NGC 1068 (Kinkhabwala *et al.* 2002*a*). Features from hydrogen- and helium-like ions from carbon to silicon, as well as significant emission due to iron L-shell transitions, dominate the spectrum of its active galactic nucleus. Bright, narrow RRC point unambiguously to the predominance of recombination in a photoionized plasma. Strong higher-order Rydberg transitions (np → 1s) are present, implying the photoexcitation contributes to the spectrum as well.

3. Hydrogen-like ions

At the characteristic temperatures of X-ray-emitting plasmas, the low-Z abundant elements (such as carbon, nitrogen and oxygen) are often found in their hydrogen-like charge states. The most prominent emission lines from hydrogen-like ions are the Lyman-series transitions:

Lyman $\alpha_{1,2}$: $2\mathrm{p}\,{}^2P_{3/2,1/2} \rightarrow 1\mathrm{s}$

Lyman $\beta_{1,2}$: $3\mathrm{p}\,{}^2P_{3/2,1/2} \rightarrow 1\mathrm{s}$

Lyman $\gamma_{1,2}$: $4\mathrm{p}\,{}^2P_{3/2,1/2} \rightarrow 1\mathrm{s}$

$\vdots$

These lines are usually quite bright, and are therefore good for abundance and velocity determinations. Examples are shown in figure 3, which displays the XMM-Newton reflection-grating spectrum of the supernova remnant (SNR) 1E0102-72.3 in the Small Magellanic Cloud (Rasmussen *et al.* 2001). This young core-collapse remnant is likely to be an oxygen-rich type-1b SNR akin to CasA (Blair *et al.* 2000), so the spectrum is dominated by lines of elements produced by α-burning reactions. The Lyman-series lines (α through γ) of hydrogen-like carbon, oxygen, neon and magnesium are clearly visible in the spectrum, as marked in the figure.

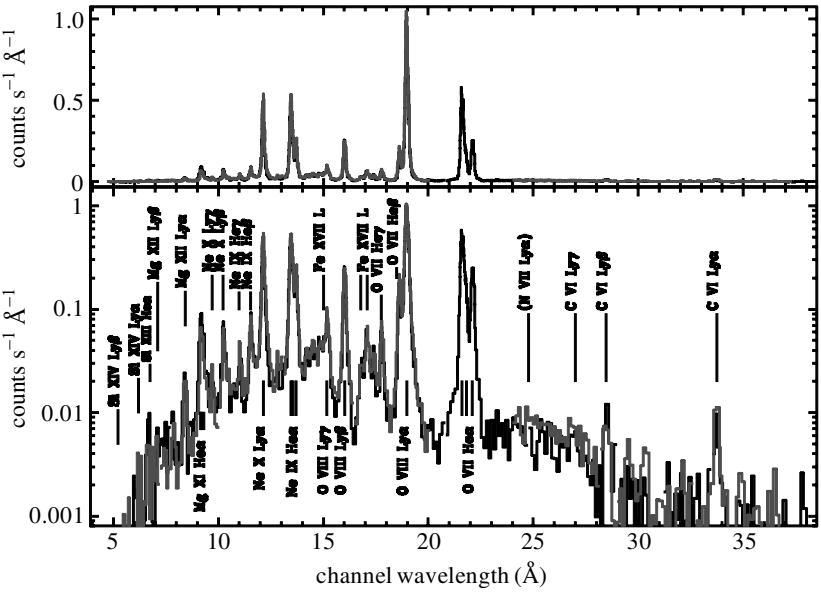

Figure 3. XMM-Newton reflection-grating spectrum of SNR 1E0102-72.3 (Rasmussen *et al.* 2001). For clarity, the spectrum is shown in both linear (top) and logarithmic units (bottom). Hydrogen- and helium-like emission lines from carbon to silicon are present with significant emission from iron L-shell transitions as well.

Despite their prominence in astrophysical X-ray spectra, Lyman-series transitions have rather limited utility as density and temperature diagnostics. Lines in this series are all produced through electric dipole transitions, so the radiative decay rates are high, and the collisional couplings are negligible. In addition, because of the n^{-2} dependence of the hydrogen-like energy levels (where n is the principal quantum number), the upper levels for the different transitions in the series are close in energy, so the Boltzmann factor in the excitation rates varies only slightly from transition to transition in the temperature range where the hydrogen-like ion is the dominant species.

At the very low temperatures characteristic of photoionized plasmas, Lyman-series lines are formed by radiative cascades associated with radiative recombination. The line ratios produced by these processes are somewhat different than those associated with collisional excitation in collisional plasmas. For example, the Lyβ-to-Lyα ratio for O^{7+} is *ca.* 0.11 for a collision-dominated plasma, while the same ratio is *ca.* 0.14 for a recombination-dominated plasma (Kinkhabwala *et al.* 2002*b*). Similar enhancements are found for the higher series line ratios as well. However, the presence of significant photoexcitation in a photoionized plasma can enhance higher series lines even more than expected for collision-dominated plasma, thereby complicating this diagnostic.

4. Helium-like ions

The helium-like K-shell lines are among the most important in X-ray spectra of cosmic sources. Since the helium-like ground state is a tight 'closed' shell, this is the dominant ion species for each element over a wide range in temperature, particularly

in collisionally ionized plasmas. In addition, as we explain below, these lines exhibit strong sensitivity to electron density, temperature and ionization conditions in the emitting plasma.

The most important K-shell helium-like transitions are as follows:

W: $1s2p\,{}^1P_1 \rightarrow 1s^2\,{}^1S_0$

X: $1s2p\,{}^3P_2 \rightarrow 1s^2\,{}^1S_0$

Y: $1s2p\,{}^3P_1 \rightarrow 1s^2\,{}^1S_0$

Z: $1s2s\,{}^3S_1 \rightarrow 1s^2\,{}^1S_0$

W is an electric dipole transition, also called the *resonance* transition, and is sometimes designated by r. X and Y are the so-called *intercombination* lines. These are usually blended (especially for the lower-Z elements), and are collectively designated by i. Z is the *forbidden* line, often designated by f. It is a relativistic magnetic-dipole transition, with a very low radiative-decay rate.

The temperature sensitivity of these lines arises as follows (Gabriel & Jordan 1969; Pradhan 1982; Porquet & Dubau 2000): since W is an electric dipole transition, the collision strength for collisional excitation of this line includes important contributions from higher-order terms in the partial wave expansion, and thus continues to increase with energy above threshold. By contrast, X and Z are both electric-dipole forbidden. The dominant term in the excitation collision strength for these transitions involves electron exchange. Therefore, their excitation collision strengths drop off strongly with energy above threshold, whereas Y remains relatively constant. As a result, the line ratio $G = (\mathrm{X} + \mathrm{Y} + \mathrm{Z})/\mathrm{W}$ is a decreasing function of electron temperature.

The density sensitivity comes from the fact that the ${}^3S_1$ level can be collisionally excited to the ${}^3P$ levels. At high enough electron density, the process successfully competes with radiative decay of the forbidden line. Therefore, the ratio

$$R = \mathrm{Z}/(\mathrm{X} + \mathrm{Y})$$

drops off above a critical density, n_c. The critical density depends strongly on Z. For C^{4+}, $n_\mathrm{c} \sim 10^9\ \mathrm{cm}^{-3}$, while, for Si^{12+}, $n_\mathrm{c} \sim 10^{13}\ \mathrm{cm}^{-3}$.

These dependencies are illustrated in figure 4, which shows the helium-like spectra of oxygen, nitrogen and carbon for two stellar coronal sources, Procyon and Capella, as measured with the Chandra low-energy transmission-grating spectrometer (Ness *et al.* 2001). The corona of Procyon is both cooler and of higher density than that of Capella. As can be seen, the forbidden line of carbon is comparatively suppressed due to the higher density in the Procyon spectrum. However, the density is not high enough to alter the oxygen lines. Here the forbidden and intercombination line intensities are comparatively greater for Procyon, because of the lower temperature.

The helium-like line ratios can also be affected by the presence of a significant ultraviolet radiation field (Gabriel & Jordan 1969). In particular, the ${}^3S_1$ level can be photoexcited to ${}^3P$ levels, prior to radiative decay, if there is sufficient ultraviolet intensity at the energy of the relevant transitions. That leads to suppression of the forbidden line and enhancement of the intercombination lines, mimicking the effects of high electron density. This process is an important contributor in the spectra of early-type stars, and some accretion-powered sources (Kahn *et al.* 2001).

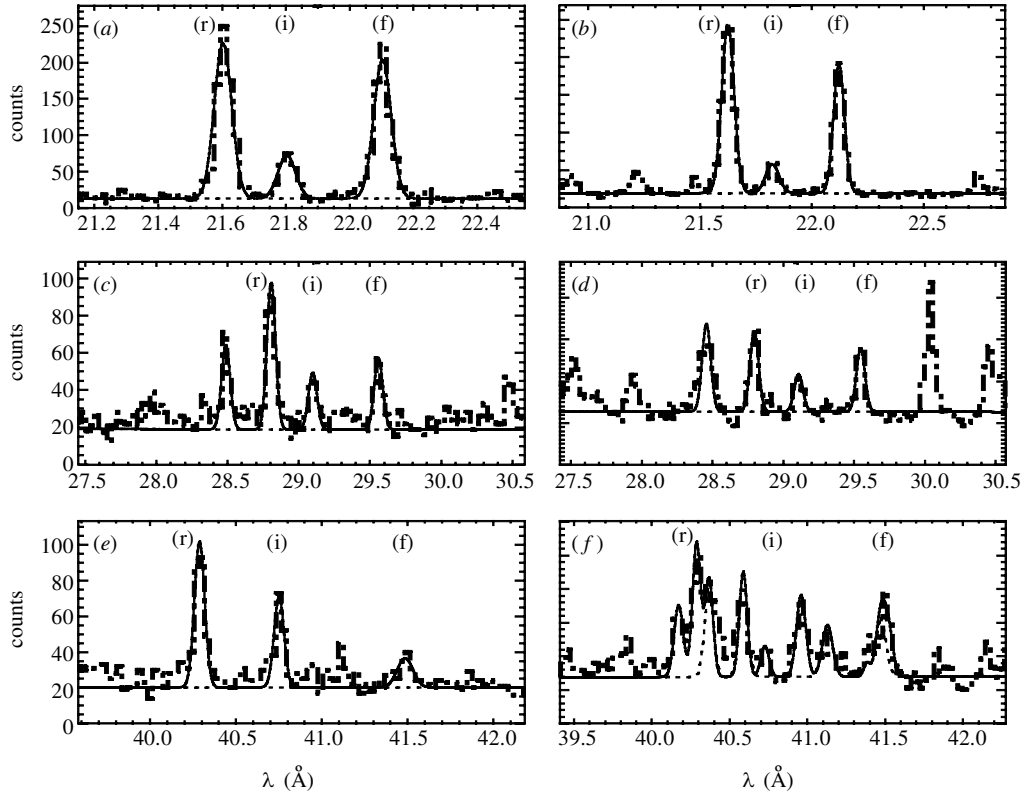

Figure 4. Helium-like triplets for O, N and C from the coronal stars Procyon and Capella (Ness *et al.* 2001). (*a*) Procyon O_{VII} triplet; (*b*) Capella O_{VII} triplet; (*c*) Procyon N_{VI} triplet; (*d*) Capella N_{VI} triplet; (*e*) Procyon C_{V} triplet; (*f*) Capella C_{V} triplet.

In photoionized plasmas, the excited levels for helium-like ions are fed directly by recombination and also by radiative cascades following recombination onto higher levels. The forbidden line is most intense, since most of the cascades from high-n and high-l (high-J) levels land on the lowest lying 1s2s ($J = 1$) level, which produces the forbidden line. This can be seen in the spectrum of NGC 1068 shown in figure 2, for both the helium-like oxygen lines near 22 Å and the helium-like nitrogen lines near 29 Å. However, if photoexcitation from the continuum is important, the resonance line can also be enhanced, partly offsetting this effect. The various contributions can be disentangled by looking at the higher series helium-like transitions (Kinkhabwala *et al.* 2002*a*, *b*). For high-density photoionized plasmas, the forbidden line is suppressed, and the intercombination lines may actually dominate the spectrum (Cottam *et al.* 2001).

5. Iron L-shell transitions

Since iron is the most abundant high-Z element, its L-shell spectrum plays a crucial role in astrophysical X-ray spectroscopy. As a result of their higher ionization potential, the iron L-shell ions contribute significant line emission even when the lower-Z elements are fully stripped. For collisionally ionized plasmas, this complex samples

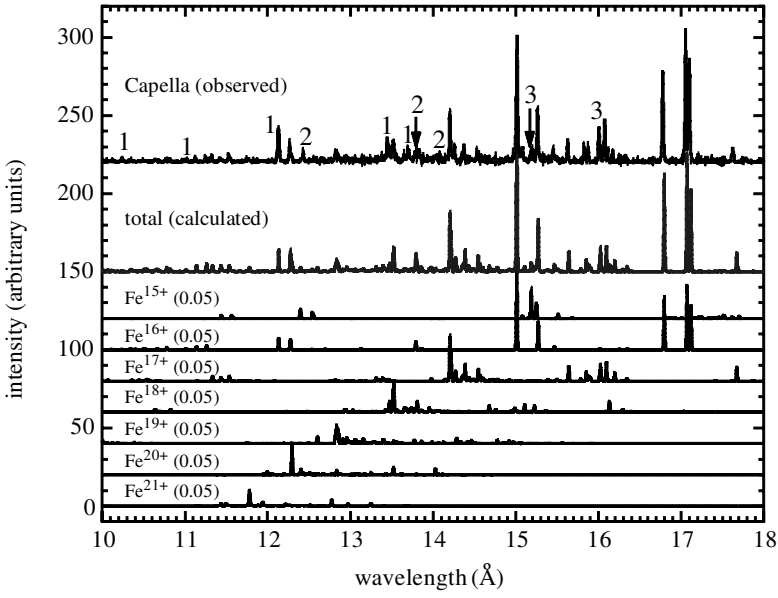

Figure 5. Observed Capella spectrum compared with the total calculated iron (only) spectrum (Behar *et al.* 2001). The seven separate plots at the bottom of the figure show the individual ion spectra of Fe^{15+} to Fe^{21+} (with fractional contributions to the total in parentheses). The spectra are calculated assuming plasma conditions of $kT_e = 600$ eV, which provides a very good agreement with the data. The non-iron lines are indicated by the numbers 1–3, corresponding, respectively, to lines of neon, nickel and oxygen.

a wide range in temperature (0.2–2 keV). In addition, the L-shell spectrum is very 'rich', and there is significant diagnostic sensitivity.

The brightest iron L-shell lines are of the form:

$$2s^2 2p^{k-1} 3d \rightarrow 2s^2 2p^k$$

$$2s^2 2p^{k-1} 3s \rightarrow 2s^2 2p^k$$

$$2s^2 p^k 3p \rightarrow 2s^2 2p^k$$

The 2p–3d lines generally have the highest oscillator strength. The line positions are a strong function of charge state. Thus, the ionization structure is easily discernible, which provides a simple, abundance-independent constraint on the temperature distribution.

This is illustrated in figure 5, which shows the iron L-spectrum of Capella, as observed with the XMM-Newton reflection-grating spectrometer. Plotted below the measured data are the calculated contributions from each of the individual charge states, ranging from sodium-like iron (Fe^{15+}) to beryllium-like iron (Fe^{21+}). Note the relatively clean separation between the L-shell complexes from each of these ions, allowing for easy decomposition of the spectrum, even with only moderate spectral resolution.

Density sensitivity arises from the fact that the intermediate iron L charge states (e.g. those that are nitrogen-like and carbon-like) possess a number of low-lying metastable levels associated with $n = 2 \rightarrow n' = 2$ excitations. These can be populated collisionally, leading to new 'seed' states for $2 \rightarrow 3$ excitations followed by

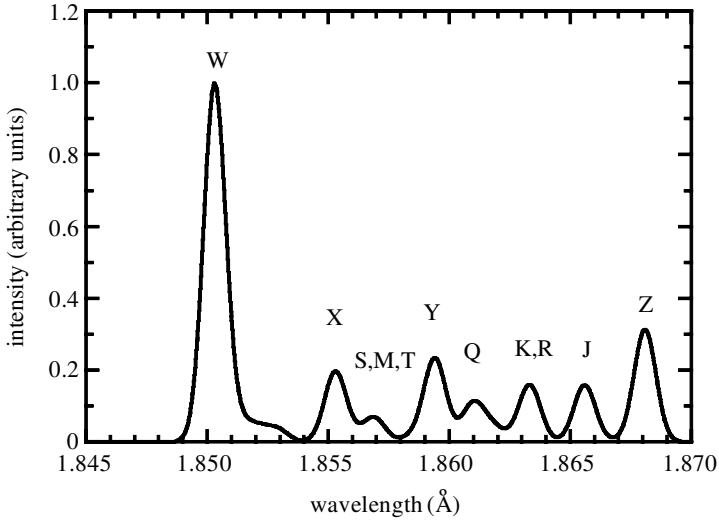

Figure 6. Synthetic iron K-spectrum at a temperature of 35 MK. Line widths are due solely to thermal broadening. Major features are labelled using the convention of Gabriel (1972). The relevant atomic data are from Bely-Dubau *et al.* (1979*a*, *b*, 1982). Wavelengths have been shifted to agree with the laboratory measurements of Beiersdorfer *et al.* (1993).

$3 \rightarrow 2$ radiative decays. Such density diagnostics 'turn on' at electron densities of *ca.* 10^{13} cm^{-3}.

6. The iron K-shell complex

The iron K complex is relatively isolated in the spectrum at energies *ca.* 6–7 keV, where even non-dispersive detectors have moderate spectral resolution (see figure 6 for a synthetic iron K-spectrum). Thus, iron K lines were the first discrete atomic features unambiguously detected for cosmic-X-ray sources (see, for example, Sanford *et al.* 1975; Pravdo *et al.* 1976; Mitchell *et al.* 1976).

An important contributor to iron K emission, especially for accretion-powered sources, is fluorescence from cold material in the vicinity of a bright X-ray continuum. Fluorescence involves a radiative decay following inner-shell photoionization, i.e. a transition of the form $1s2s^22p^k nl \rightarrow 1s^22s^22p^{k-1}nl$. The excited level, in this case, can also decay via autoionization by ejecting one of the outer electrons in the valence shell. This latter process dominates for low-Z elements. However, since radiative decay rates scale like Z^4 and autoionization decay rates scale like Z^0 (e.g. Cowan 1981), the fluorescence yield becomes appreciable for a high-Z element like iron. The near-neutral iron K fluorescence line falls at 6.4 keV, easily distinguishable from the helium-like lines near 6.7 keV and the Lyman α line at 7.1 keV.

The iron K complex also exhibits new features due to the relative importance of dielectronic recombination (DR). DR leads to lithium-like 'satellites' to helium-like K-lines: $1s2pnl \rightarrow 1s^2nl$. These satellites are shifted down in energy. Higher n implies a smaller shift, and is associated with a higher energy of the recombining electron. Therefore, the satellite spectrum is temperature sensitive (Dubau & Volonte 1980).

At astrophysical densities, all atoms are in the ground state. Most of the satellite lines cannot be produced by collisional excitation of lithium-like iron (e.g. $1s2p^2 \rightarrow$

$1s^2 2p$). They come purely from DR on helium-like atoms. However, other lines terminate in the ground configuration of the lithium-like ion (e.g. $1s2s2p \rightarrow 1s^2 2s$). These can be produced by both collisional excitation of lithium-like atoms and DR on helium-like atoms. Hence, the line ratios for these various transitions provide an independent measure of the charge balance. Analysis of the iron K helium-like spectrum thus provides independent constraints on the electron temperature and the level of ionization, and is ideal for investigating departures from ionization equilibrium.

7. Summary

X-ray spectroscopy provides a unique and powerful new avenue of investigation for the study of a wide range of astrophysical sources. Discrete X-ray line diagnostics can be used to provide unambiguous measurements of temperatures, densities, excitation conditions, ionization balance and elemental abundances. Many of these techniques have already been employed in the analysis and interpretation of data acquired by the grating experiments on Chandra and XMM-Newton, especially at soft-X-ray energies. This field is still in its infancy. There are undoubtedly many surprises yet to come.

References

Behar, E., Cottam, J. & Kahn, S. M. 2001 *Astrophys. J.* **548**, 966.

Beiersdorfer, P., Phillips, T., Jacobs, V. L., Hill, K. W., Bitter, M., von Goeler, S. & Kahn, S. M. 1993 *Astrophys. J.* **409**, 846.

Bely-Dubau, F., Gabriel, A. H. & Volonté, S. 1979*a* *Mon. Not. R. Astron. Soc.* **186**, 405.

Bely-Dubau, F., Gabriel, A. H. & Volonté, S. 1979*b* *Mon. Not. R. Astron. Soc.* **189**, 801.

Bely-Dubau, F., Dubau, J., Faucher, P. & Gabriel, A. H. 1982 *Mon. Not. R. Astron. Soc.* **198**, 239.

Blair, W. P., Morse, J. A., Raymond, J. C., Kirshner, R. P., Hughes, J. P., Dopita, M. A., Sutherland, R. S., Long, K. S. & Winkler, P. F. 2000 *Astrophys. J.* **537**, 667.

Brinkman, A. C. *et al.* 2000 *Astrophys. J.* **530**, L111.

Canizares, C. R. *et al.* 2000 *Astrophys. J.* **539**, L41.

Cottam, J. C., Kahn, S. M., Brinkman, A. C., den Herder, J. W. & Erd, C. 2001 *Astron. Astrophys.* **365**, L277.

Cowan, R. D. 1981 *The theory of atomic stucture and spectra.* Berkeley, CA: University of California Press.

den Herder, J. W. *et al.* 2001 *Astron. Astrophys.* **365**, L7.

Dubau, J. & Volonte, S. 1980 *Rep. Prog. Phys.* **43**, 199.

Gabriel, A. H. 1972 *Mon. Not. R. Astron. Soc.* **160**, 99.

Gabriel, A. H. & Jordan, C. 1969 *Mon. Not. R. Astron. Soc.* **145**, 241.

Giacconi, R., Gursky, H., Paolini, F. & Rossi, B. B. 1962 *Phys. Rev. Lett.* **9**, 439.

Kahn, S. M. *et al.* 2001 *Astron. Astrophys.* **365**, L312.

Kallman, T. & Bautista, M. 2001 *Astrophys. J. Suppl.* **133**, 221.

Kinkhabwala, A., Sako, M., Behar, E., Kahn, S. M., Paerels, F., Brinkman, A. C., Kaastra, J. S., Gu, M. F., Liedahl, D. A. 2002*a*. (In preparation.)

Kinkhabwala, A., Behar, E., Sako, M., Gu, M. F., Kahn, S. M. & Paerels, F. 2002*b*. (In preparation.)

Liedahl, D. A. 1999 In *X-ray spectroscopy in astrophysics* (ed. J. van Paradijs & J. A. M. Bleeker), p. 189. Springer.

Mazzotta, P., Mazzitelli, G., Colafrancesco, S. & Vittorio, N. 1998 *Astrophys. J. Suppl.* **133**, 403.

Mitchell, R. J., Culhane, J. L., Davison, P. J. & Ives, J. C. 1976 *Mon. Not. R. Astron. Soc.* **175**, 29.

Ness, J.-U. *et al*. 2001 *Astron. Astrophys.* **367**, 282.

Porquet, D. & Dubau, J. 2000 *Astrophys. J. Suppl.* **143**, 495.

Pounds, K. 2002 *Phil. Trans. R. Soc. Lond.* A **360**, 1905–1921.

Pradhan, A. K. 1982 *Astrophys. J.* **263**, 477.

Pravdo, S. H. *et al*. 1976 *Astrophys. J.* **206**, L41.

Rasmussen, A. P., Behar, E., Kahn, S. M., den Herder, J. W. & van der Heyden, K. 2001 *Astron. Astrophys.* **365**, L231.

Sanford, P., Mason, K. O. & Ives, J. 1975 *Mon. Not. R. Astron. Soc.* **173**, 9.